




## Article

# Analytical and Numerical Study on the Performance of the Curved Surface of a Circular Tunnel Reinforced with CFRP

Fan Yang <sup>1</sup>, Gan Qin <sup>2,\*</sup>, Kang Liu <sup>1</sup>, Feng Xiong <sup>1</sup> and Wu Liu <sup>1,\*</sup><sup>1</sup> School of Civil Engineering, Hefei University of Technology, Hefei 230009, China<sup>2</sup> Shenzhen Urban Public Safety and Technology Institute, Shenzhen 518046, China

\* Correspondence: qingan@szsti.org (G.Q.); liuwu168@hfut.edu.cn (W.L.)

**Abstract:** Pasting carbon fiber reinforced polymer (CFRP) has become an effective method to reinforce the circular tunnel. For this reinforcement method, the mechanical performance of the curved substrate is important to keep the coordinated deformation of CFRP and the lining concrete. To investigate the effect of interface curvature on the stresses of the reinforced interface, an analytical model is proposed for the curved reinforced interface with the consideration of the interface bond–slip relationship. Additionally, a 3D numerical model is established to further investigate the effects of some important parameters (CFRP’s layer, length, elastic modulus, thickness and the adhesive’s elastic modulus, thickness) on the reinforced interface stresses. The results reveal that the stress state of the curved reinforced interface is more complex than that of the plane reinforced interface. With decreasing the radius of the curved reinforced interface, the interface radial stresses are increased significantly, while the circumferential stresses hardly change. For the adhesive, decreasing the elastic modulus and thickness of the adhesive layer can significantly improve the stress state of the reinforced interface. For the CFRP, decreasing the thickness, elastic modulus and layer number of CFRP is conducive to full utilization of materials and long-term combined work of the concrete and CFRP.

**Keywords:** tunnel reinforcement; CFRP; curved interface; interface stress; finite element model



**Citation:** Yang, F.; Qin, G.; Liu, K.; Xiong, F.; Liu, W. Analytical and Numerical Study on the Performance of the Curved Surface of a Circular Tunnel Reinforced with CFRP. *Buildings* **2022**, *12*, 2042. <https://doi.org/10.3390/buildings12112042>

Academic Editors: Shan Gao, Jingxuan Wang, Dewen Kong and Yong Liu

Received: 19 October 2022

Accepted: 18 November 2022

Published: 21 November 2022

**Publisher’s Note:** MDPI stays neutral with regard to jurisdictional claims in published maps and institutional affiliations.



**Copyright:** © 2022 by the authors. Licensee MDPI, Basel, Switzerland. This article is an open access article distributed under the terms and conditions of the Creative Commons Attribution (CC BY) license (<https://creativecommons.org/licenses/by/4.0/>).

## 1. Introduction

Circular tunnels are usually buried deep in a complex environment. After a period of operation, quality defects such as lining cracks and water leakage are prone to appear. The existence of the above defects will inevitably deteriorate the stress of the lining structure and lead to unfavorable conditions, such as stress concentration and excessive deformation, which will have a negative impact on the safety of the whole tunnel project in some serious cases [1]. At the same time, with the rapid development of urban construction, the external conditions of the tunnels are also constantly changing, including the construction of upper roads, high-speed railways, high-rise buildings, upper ponds, and various new infrastructures. These changes in the external conditions have a potential impact on the tunnel, which may make the lining structures treacherous [2]. Once the external conditions are changed and cannot meet the requirements for the tunnel safety and stability, it is necessary to adopt some corresponding reinforcement schemes for the lining structures.

The technology of carbon fiber reinforced polymer (CFRP) reinforcement in concrete structures was first studied by the Swiss Federal Laboratories for Materials, which used the method of applying CFRP in the reinforcement of the Ibach bridge and achieved good reinforcement results [3]. Subsequently, this CFRP reinforcement technology was widely applied in various structural reinforcements because of the good mechanical properties of CFRP and high construction efficiencies, such as compressive or seismic reinforcement of concrete columns [4–6] and the reinforcement of various beam and slab structures [7]. The successful application of CFRP reinforcement technology in the field of civil building reinforcement has also inspired engineers and technicians to continuously explore the

possibility and effectiveness of CFRP reinforcement technology in the field of hydraulic tunnel lining. Since CFRP is characterized by high strength, stable performance, corrosion resistance and light weight [8,9], it can effectively control the continual expansion of lining cracks and prevent the lining from falling off and spalling, which was well applied in the circular hydraulic tunnels of Taohua River Reservoir, Qingshan Reservoir and Dahuofang Reservoir [10]. When the concrete is reinforced with CFRP, the CFRP contributes to the structural strength, mainly by bearing the stress transferred from the reinforced interface. Therefore, many researchers focus on the mechanical properties of the interface between CFRP and concrete by experimental and analytical methods. For the experimental methods, some single shear tests [11–13] and double shear tests [14] were performed to obtain the stress–slip relationship of the reinforced interface. Additionally, in-plane shear tests are also important methods to obtain the bond–slip constitutive models of the reinforced interface, and based on these tests, the Neubauer and Rostasy model [15], Monti model [16], Nakaba model [17] and Savioa model [18] are proposed. For analytical methods, the elastic mechanic method is a common method to calculate the interface stress between CFRP and concrete, such as the stage analytical method [19,20], considering the deformation compatibility method [21–24]. The above analytical methods are mainly based on two assumptions: the reinforcement materials are linear elastic and the interfacial stresses are constants along the direction of the adhesive thickness. Once the above two assumptions are not considered, the interfacial stresses are difficult to solve or to express explicitly [25,26].

In addition, the existing research mainly focuses on concrete beams reinforced with CFRP to improve their bending or shear resistance, the main contents are related to the shear behavior and peel failure of the reinforced interface. For these structures, the reinforced interfaces are mostly planes, and the bond stresses of the interface are mainly shear stresses [27]. However, for the circular tunnel reinforced with CFRP, the reinforced interfaces are mostly a concave curved surface, such as the reinforced concrete (RC) arch in Figure 1. Due to the existence of the interface curvature, this reinforced structure will be more prone to peel failure [28]. Therefore, the above research cannot be directly used to analyze the mechanical properties of the curved interface for circular tunnels reinforced with CFRP.

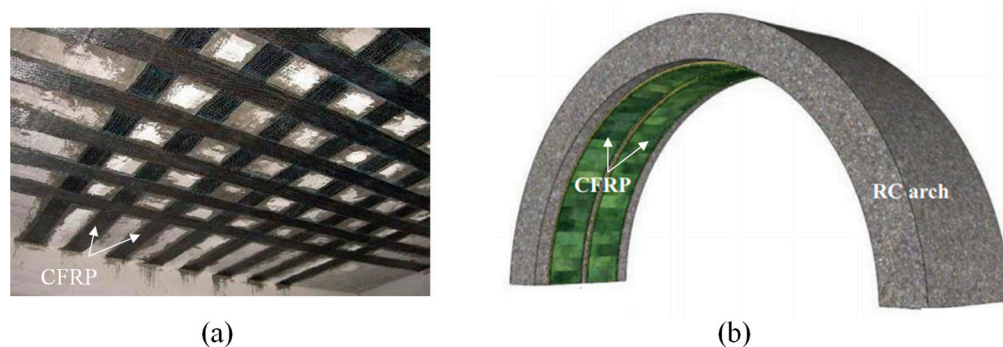


**Figure 1.** Reinforced interface: (a) plane surface; (b) concave curved surface.

Therefore, to investigate the reinforced interface stress of the circular tunnel reinforced with CFRP, an analytical model is proposed for the interaction between CFRP, adhesive and the lining concrete, and the analytical expression of the interface stress is derived with the consideration of the bond–slip at the reinforced interface. According to the analytical model, the influence of the curvature on the interface peel failure is analyzed, and the key parameters affecting the stresses of the curved reinforced interface are obtained. Subsequently, a detailed three-dimensional numerical model, which is verified by the experimental results, is established for a circular tunnel reinforced with CFRP. Based on the numerical model, the influence of the key parameters on the stresses of the curved reinforced interface is further analyzed.

## 2. Analytical Study on the Stresses of the Curved Reinforced Interface

### 2.1. Analytical Model

As shown in Figure 2, an analytical model is proposed for the curved reinforced interface of a circular tunnel reinforced with CFRP. The thickness of CFRP is  $t_c$ , the elastic modulus of CFRP is  $E_c$ , and the pasted length of CFRP is  $L$ , the thickness of the adhesive layer is  $t_a$ , the elastic modulus of the adhesive layer is  $E_a$ , the radius of the curved interface is  $r$ . A force ( $F$ ) is applied to the CFRP along the tangential direction. The stress condition of an infinitesimal section is presented in Figure 2b.

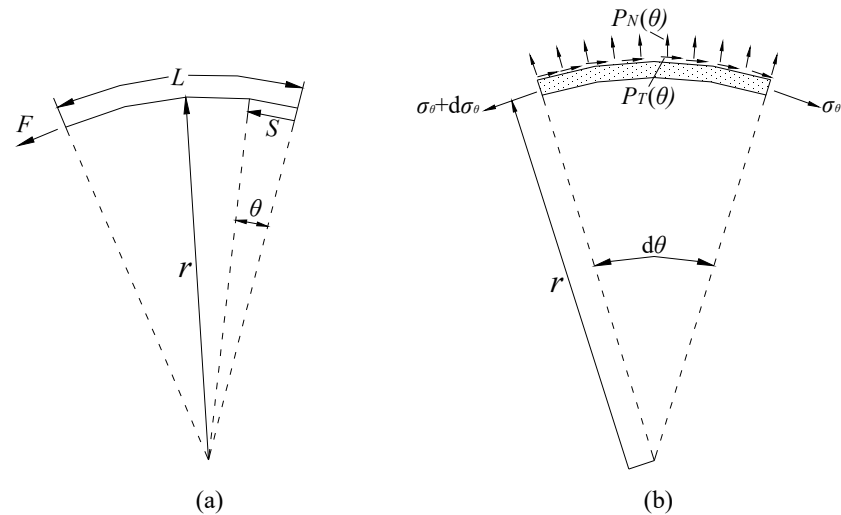


**Figure 2.** Analytical model: (a) curved reinforced interface dimensions; (b) infinitesimal section.

To simplify the calculation, the CFRP and adhesive can be simplified as a layer of reinforcement material [29], and the equivalent thickness is:

$$t = t_c + t_a \quad (1)$$

The equivalent elastic modulus of the reinforcement material can be calculated by:

$$E = \frac{E_c E_a}{E_c + E_a} \quad (2)$$

The circumferential stress of the reinforcement material is  $\sigma_\theta$ , the distance from the calculated point to the free end is  $s$ , and the radial and tangential stresses of the reinforced interface are  $P_N$  and  $P_T$ , respectively. As shown in Figure 2b, the equilibrium equations of the infinitesimal section can be expressed as:

$$P_T \times ds = t \times d\sigma_\theta \quad (3)$$

$$P_N \times r \times d\sigma_\theta = (\sigma_\theta + d\sigma_\theta + \sigma_\theta) \times t \times \sin \frac{d\sigma_\theta}{2} \quad (4)$$

According to Hook's law, the stress–strain relationship of the reinforcement material can be obtained by:

$$\sigma_\theta = E \varepsilon_\theta \quad (5)$$

Substitute Equation (5) into Equations (3) and (4), we obtain:

$$P_T = Et \frac{d\varepsilon_\theta}{ds} \quad (6)$$

$$P_N = \frac{Et}{r} \varepsilon_\theta \quad (7)$$

The relative tangential slip ( $g_T$ ) and radial slip ( $g_N$ ) at the interface between the adhesive and concrete can be defined by the following equations.

$$g_T = u_\theta - u_{\theta,s} \quad (8)$$

$$g_N = u_r - u_{r,s} \quad (9)$$

where  $u_\theta$  is the tangential displacement of the adhesive at the interface between the adhesive and the concrete,  $u_{\theta,s}$  is the tangential displacement of the concrete at the interface between the adhesive and the concrete;  $u_r$  is the radial displacement of the adhesive at the interface between the adhesive and the concrete,  $u_{r,s}$  is the radial displacement of the concrete at the interface between the adhesive and the concrete. Since the deformation of the concrete is much smaller than that of the adhesive the values of  $u_{\theta,s}$  and  $u_{r,s}$  are much smaller than those of  $u_\theta$  and  $u_r$ , and they can be neglected in the analytical model [30].

The relationship between the interface stress and the interface slip can be obtained by:

$$P_T = k_T g_T \quad (10)$$

$$P_N = k_N g_N \quad (11)$$

where  $k_T$  is the tangential stiffness of the interface, and  $k_N$  is the radial stiffness of the interface. According to Equations (6) to (11), we obtain:

$$k_T u_\theta = Et \frac{d\varepsilon_\theta}{ds} \quad (12)$$

$$k_N u_r = \frac{Et}{r} \varepsilon_\theta \quad (13)$$

The geometric equation in the polar coordinate is:

$$\varepsilon_\theta = \frac{du_\theta}{ds} + \frac{u_r}{r} \quad (14)$$

Substituting Equation (14) into Equations (12) and (13), we obtain:

$$k_T u_\theta = Et \left( \frac{d^2 u_\theta}{ds^2} + \frac{1}{r} \frac{du_r}{ds} \right) \quad (15)$$

$$k_N u_r = \frac{Et}{r} \left( \frac{du_\theta}{ds} + \frac{u_r}{r} \right) \quad (16)$$

According to Equation (16),

$$u_r = \frac{Etr}{k_N r^2 - Et} \frac{du_\theta}{ds} \quad (17)$$

Substituting Equation (17) into Equation (15), we obtain:

$$\frac{d^2 u_\theta}{ds^2} - \frac{k_T}{Et} \left( 1 - \frac{Et}{k_N r^2} \right) u_\theta = 0 \quad (18)$$

We define a variable by:

$$\lambda^2 = \frac{k_T}{Et} \left( 1 - \frac{Et}{k_N r^2} \right) \quad (19)$$

Substituting Equation (19) into Equation (18), we obtain:

$$\frac{d^2 u_\theta}{ds^2} - \lambda^2 u_\theta = 0 \quad (20)$$

According to Equations (20) and (17),  $u_\theta$  and  $u_r$  can be expressed as:

$$u_\theta = A_1 \sinh(\lambda s) + A_2 \cosh(\lambda s) \quad (21)$$

$$u_r = \frac{Etr}{k_N r^2 - Et} (A_1 \cosh(\lambda s) + A_2 \sinh(\lambda s)) \quad (22)$$

where  $A_1$  and  $A_2$  are the constants to be determined by the boundary conditions. Substituting Equations (21) and (22) into Equation (14),  $\varepsilon_\theta$  can be calculated by:

$$\varepsilon_\theta = \frac{k_N r^2}{k_N r^2 - Et} \lambda (A_1 \cosh(\lambda s) + A_2 \sinh(\lambda s)) \quad (23)$$

As the analytical model shows in Figure 2a, the boundary conditions are:

$$\varepsilon_\theta(0) = 0 \quad (24)$$

$$\varepsilon_\theta(L) = \frac{F}{Et} \quad (25)$$

According to Equations (23) to (25), the constants can be obtained:

$$A_1 = 0 \quad (26)$$

$$A_2 = \frac{F\lambda}{k_T \sinh(\lambda L)} \quad (27)$$

Substituting Equations (26) and (27) into Equations (21) and (22),  $u_\theta$  and  $u_r$  can be calculated by:

$$u_\theta = \frac{F\lambda}{k_T \sinh(\lambda L)} \cosh(\lambda s) \quad (28)$$

$$u_r = \frac{F\lambda}{k_N r \sinh(\lambda L)} \sinh(\lambda s) \quad (29)$$

According to Equations (10), (11), (28) and (29), the interface radial stress ( $P_T(s)$ ) and the interface circumferential stress ( $P_N(s)$ ) can be obtained by Equations (30) and (31), separately.

$$P_T(s) = \frac{F\lambda}{\sinh(\lambda L)} \cosh(\lambda s) \quad (30)$$

$$P_N(s) = \frac{F}{r \sinh(\lambda L)} \sinh(\lambda s) \quad (31)$$

## 2.2. Effect of the Curvature on Interface Stresses

Based on Equations (30) and (31), the effects of the interface curvature on the reinforced interface stresses are investigated. The involved parameters and load in the analytical model are presented in Table 1, and the calculated interface stresses are presented in Figure 3.

**Table 1.** Parameters and load.

Parameter	$E_a$	$t_a$	$E_c$	$t_c$	$L$	$F$
Value	2 GPa	1 mm	250 GPa	0.111 mm	150 mm	50 N/m

Figure 3a presents that the interface curvature has little influence on the interface circumferential stresses. However, according to Figure 3b, the interface radial stresses are significantly influenced by the interface curvature. Obviously, with decreasing the interface curvature radius, the interface radial stresses tend to be increased, which is unfavorable for protecting the reinforced interface from peel failure.

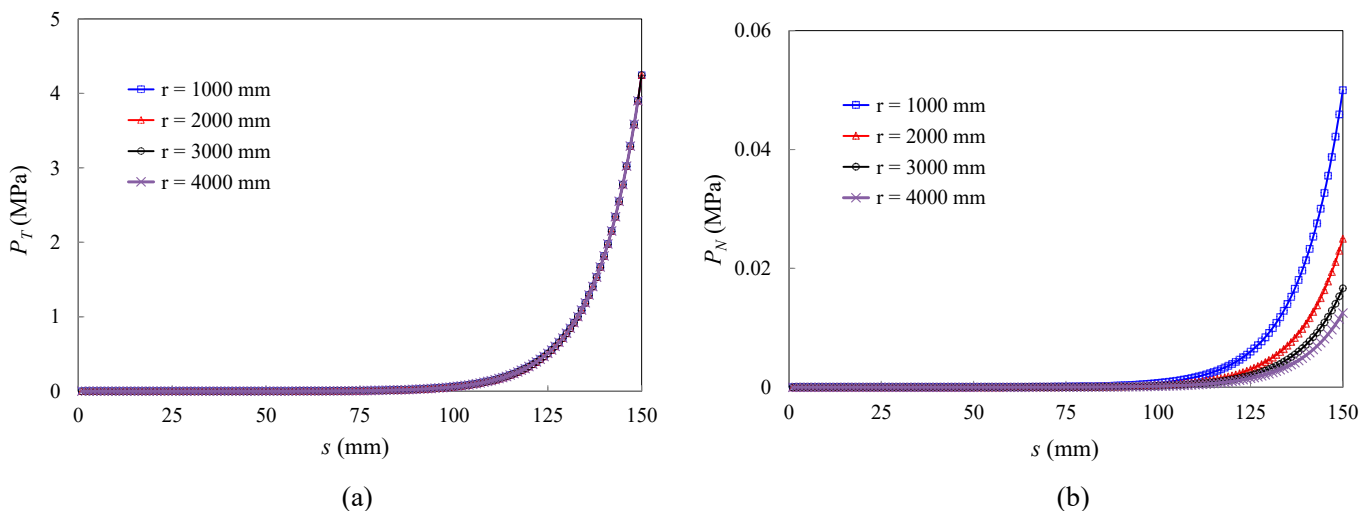


Figure 3. Analytical results of the interface stresses: (a) circumferential stress; (b) radial stress.

For the concrete beams or columns reinforced with CFRP, the reinforced interface is mostly flat and mainly in a pure shear state (State A), as shown in Figure 4. For the circular tunnel reinforced with CFRP on the internal surface, the reinforced interface is a curved surface. The analytical results show that the existence of interface curvature causes not only circumferential stresses (State A) but also radial stresses (State B) to exist on the curved reinforced interface. Therefore, the interface stress state (State C) of the curved reinforced interface is more complex than that of the plane interface.

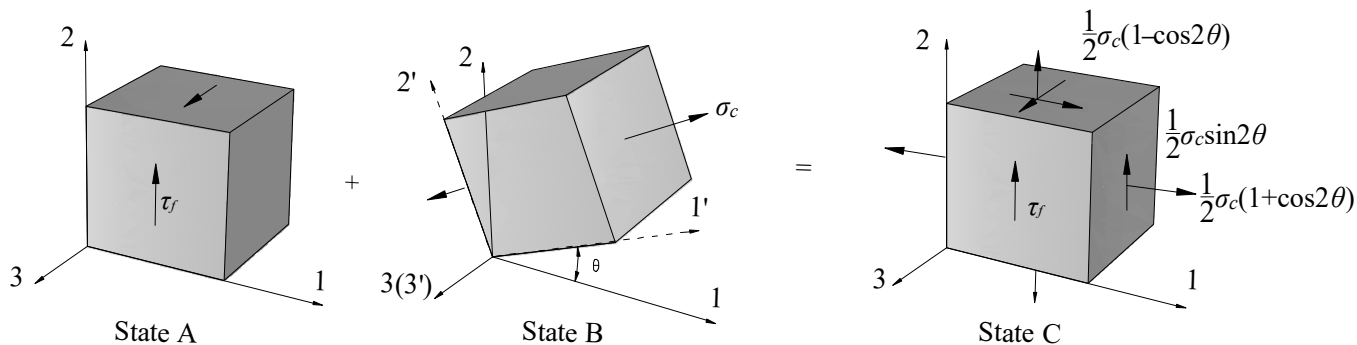


Figure 4. Stress state of the reinforced interface: State A pure shear state; State B radial stress state; State C interface stress state.

### 2.3. Effect of the Stress State on Peel Failure

When the principal stress of the concrete cover exceeds the tensile strength of the concrete, the reinforced interface exhibits peel failure. Therefore, the peel stress can be expressed as:

$$\sigma_b = \frac{P_N}{2} + \sqrt{\left(\frac{P_N}{2}\right)^2 + P_T^2} \tag{32}$$

For the interface radial stress, the positive value represents the curved reinforced interface between the adhesive and lining concrete, which is in tension, and the negative value represents the curved reinforced interface between the adhesive and lining concrete, which is in compression. For the interface circumferential stress, the positive value and negative value represent two opposite shear directions. For a circular tunnel reinforced with CFRP, the stress states of the concrete cover can be divided into two cases. (1) The interface of the concrete cover is in radial compression and circumferential shear. According to Equation (32), in this case, whether the peeling failure occurs is mainly determined by

the circumferential shear stress  $P_T$ , and the existence of radial compressive stress  $P_N$  is beneficial to prevent the interface from experiencing peel failure. (2) The interface of the concrete cover is in radial tension and circumferential shear. According to Equation (32), this case is the most unfavorable condition, and the existence of the radial tensile stress will further increase the reinforced interface stresses, which will lead to earlier peel failure of the structure.

To decrease the radial tensile stresses of the reinforced interface that have a negative effect on this composite structure, some material parameters and construction schemes should be optimized. According to Equations (30) and (31), the interface stresses are mainly affected by several parameters such as the CFRP's length ( $L$ ), layer ( $n$ ), thickness ( $t_c$ ), elastic modulus ( $E_c$ ), and the adhesive's thickness ( $t_a$ ), elastic modulus ( $E_a$ ). For the CFRP, it is generally divided into high-strength CFRP and high-elastic CFRP, for which the thicknesses and the elastic moduli are quite different. In addition, since the types of the adhesive are diverse, the elastic moduli are quite different. Additionally, the thickness of the adhesive layer can also be affected by the brushing operation and circumstances. Therefore, it is necessary to further investigate the effects of  $L$ ,  $n$ ,  $t_c$ ,  $E_c$ ,  $t_a$  and  $E_a$  on the stress state of the curved reinforced interface, on the basis of a practical example.

Since the factors that affect the performance of the tunnel reinforced with CFRP are complex and diverse, the analytical model is mainly used for qualitative analysis, that is, to find out the main factors. However, the analytical model is somewhat simplified. For example, the bonding slip between the adhesive layer and the liner concrete is ignored. Therefore, based on the analytical results, detailed experimental or numerical studies should be conducted for quantitative analysis to reveal the influence of these factors on the performance of the tunnel reinforced with CFRP.

### 3. Experimental Study on a Tunnel Reinforced with CFRP

The effect of a CFRP reinforcement scheme for a circular tunnel with vertical loads is preliminarily investigated by comparing the experimental results of the specimen reinforced with CFRP and the specimen without any reinforcement scheme [31]. The dimensions of the specimen are presented in Figure 5, the internal diameter is 300 mm, the thickness is 30 mm, and the longitudinal length is 1000 mm. Six rebars with a diameter of 4 mm are erected in the longitudinal direction for the concrete, and the rebars are arranged at an interval of  $60^\circ$  along the circumferential direction. In addition, spiral stirrups with a diameter of 3 mm are used in the circumferential direction, and the spacing of the spiral stirrups is 74 mm.

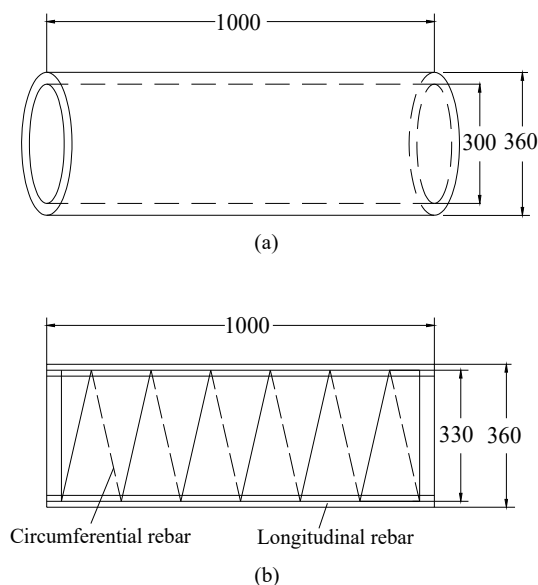


**Figure 5.** Specimen dimensions: (a) concrete; (b) rebars (mm).

The loading condition of the experimental test is shown in Figure 6. The involved materials are presented in Table 2. To investigate the stresses and strains of the concrete and CFRP, as shown in Figure 6b, several strain gauges are arranged on the internal surfaces of the concrete and CFRP.

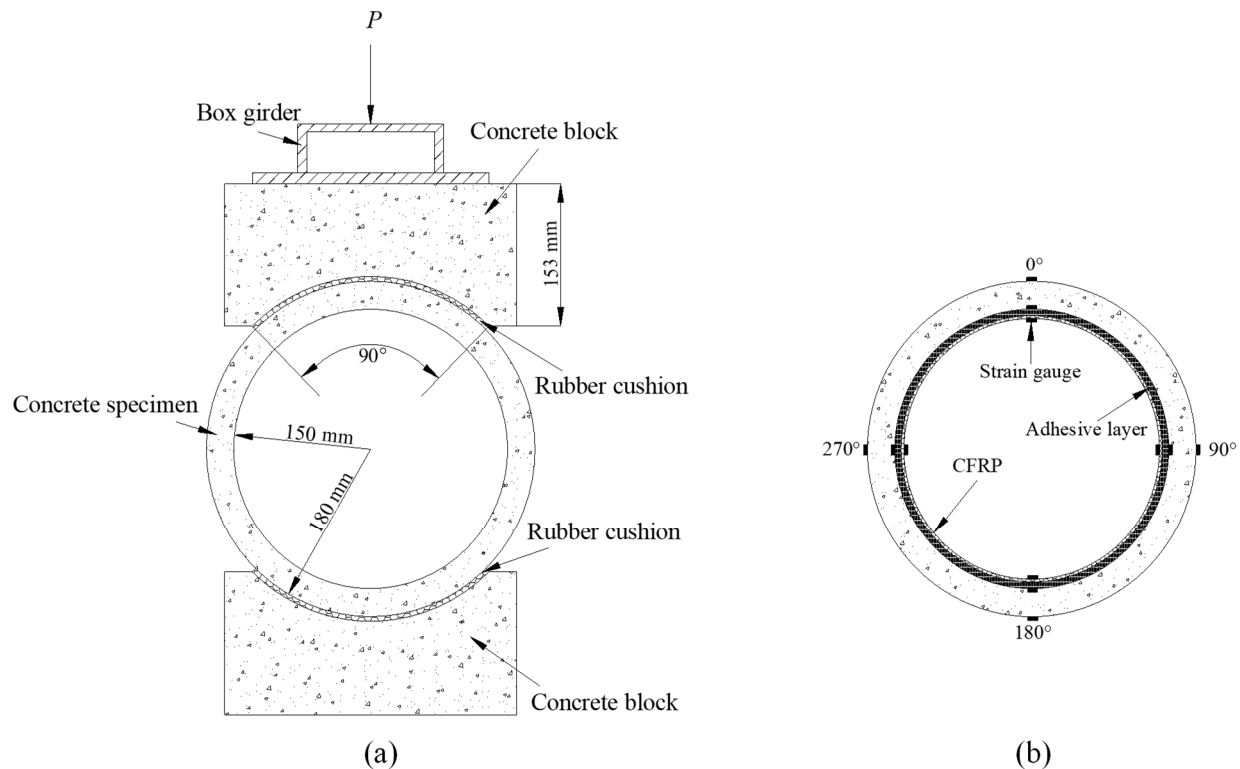


**Figure 6.** Details of the experimental test: (a) device; (b) strain gauge positions.

**Table 2.** Materials.

Material	Elastic Modulus (GPa)	Poisson's Ratio	Density (kg/m <sup>3</sup> )
C30 concrete	30	0.167	2400
Longitudinal rebar	210	0.3	7850
Circumferential rebar	210	0.3	7850
Rubber cushion	7.8	0.48	1200
CFRP	235	0.28	—
Adhesive layer	2.5	0.35	—

## 4. Numerical Simulation and Validation

### 4.1. Numerical Model

The experimental test is reproduced by the numerical software ANSYS, and the 3D finite element model is presented in Figure 7. The concrete and the adhesive are simulated by Solid 65 elements and Solid 45 elements separately; the CFRP is simulated by Shell 63 elements, and the rebar is simulated by Link 8 elements. The multilinear isotropic hardening material model is used for the concrete, the bilinear kinematic hardening material model is used for the steel, and the linear elastic model is used for the CFRP and adhesive.



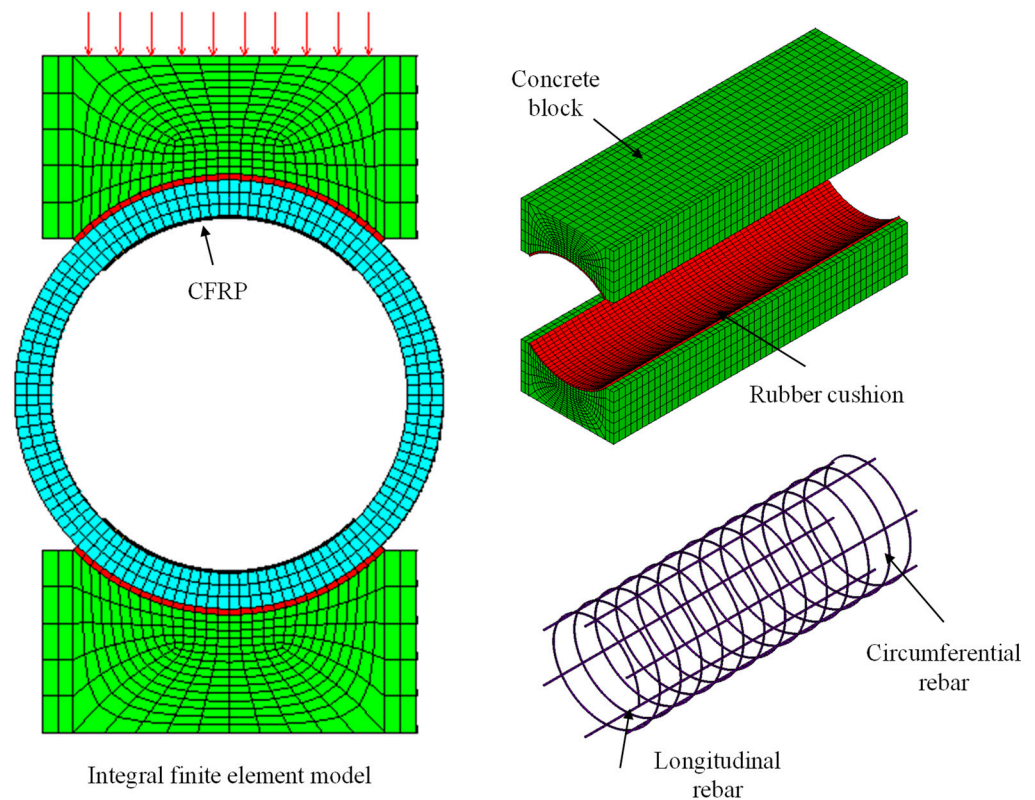


**Figure 7.** Numerical model.

The performance parameters of the adhesive layer are shown in Table 3. The spring elements (Combine 39) are used to simulate the bonding and slipping behavior of the contact interface between the adhesive layer and the concrete lining [32,33]. One end of the spring is connected to the node of the adhesive element, and the other end is connected to the node of the concrete element. The stiffness of each spring is the first-order inverse of the force-displacement relationship curve, which can be calculated as shown in Equations (33)–(36) [10,30].

$$K_{st} = \frac{dF_T}{dg_T} \quad (33)$$

$$F_T = P_T \times A_i \quad (34)$$

$$K_{sn} = \frac{dF_N}{dg_N} \quad (35)$$

$$F_N = P_N \times A_i \quad (36)$$

where  $K_{st}$  is the stiffness of the tangential spring;  $K_{sn}$  is the stiffness of the radial spring;  $A_i$  is the force area represented by each spring at the interface.

**Table 3.** Performance parameters of the adhesive layer.

Performance Items		Performance Requirements	
		Grade A Adhesive	Grade B Adhesive
Adhesive layer performance	Tensile strength (MPa)	≥40	≥30
	Modulus of elasticity under tension (MPa)	≥2500	≥1500
	Elongation rate (%)		≥1.5
	Flexural strength (MPa)	≥50	≥40
Bonding capacity	Compressive strength (MPa)		≥70
	Positive tensile bond strength with concrete (MPa)		≥2.5

Full constraints are applied to the bottom of the model, normal constraints are applied to the front and rear of the model, and the upper part of the model is free. The whole model contains 57,000 Solid 65 elements, 1758 Link 8 elements, 3000 Solid 45 elements and 18,360 Combin 39 elements. The main loads considered in the calculation include the top vertical load and the gravity. The sequence of the load application and calculation process is as follows. (1) Establish the finite element model; (2) “Kill” the adhesive elements and CFRP elements, apply the gravity and calculate; (3) Perform restart analysis, “alive” the adhesive elements and CFRP elements, apply the top vertical load and calculate.

#### 4.2. Validation

As presented in Table 4, with the vertical load of 20 kN, the circumferential micro-strains of the concrete and CFRP at 90° are obtained by the numerical simulation and compared with the experimental results. For the concrete micro-strain, the average difference between the numerical results and experimental results is within 10%. For the CFRP micro-strain, since the adhesive layer and CFRP are simplified as linear elastic materials, the differences between the numerical results and experimental results are relatively large, and the average difference is about 17%. Since the numerical results generally agree well with the experimental results, the 3D numerical model is verified, and then we can use this verified 3D numerical model to perform the following extended parameter analysis.

**Table 4.** Comparison between the experimental results and analytical results.

Force (kN)	Concrete Strain			CFRP Strain		
	Experimental Results (10 <sup>-6</sup> )	Numerical Results (10 <sup>-6</sup> )	Differences	Experimental Results (10 <sup>-6</sup> )	Numerical Results (10 <sup>-6</sup> )	Differences
5	−22.20	−23.02	3.7%	−23.39	−23.37	−0.1%
10	−45.14	−42.96	−4.8%	−53.12	−46.76	−12.0%
15	−68.08	−62.02	−8.9%	−82.86	−70.15	−15.3%
20	−91.03	−82.84	−9.0%	−112.59	−93.54	−16.9%

### 5. Parametric Study

According to the analytical study in Section 2, the interface stresses are mainly affected by  $L$ ,  $n$ ,  $t_c$ ,  $E_c$ ,  $t_a$  and  $E_a$ . Based on the numerical model, the affecting degrees of these parameters on the interface stresses are further investigated. According to some engineering practices [9,34,35], the ranges of these parameters are listed in Table 5.

**Table 5.** Parameter values.

Parameter	Reference Value	Discussion Value
$L$	180°	30°, 60°, 90°, 120°
$E_a$	2 GPa	0.24, 2, 11.2
$t_a$	2 mm	1, 2, 4
$E_c$	235 GPa	100, 300, 500
$t_c$	0.1 mm	0.1, 0.15, 0.2
$n$	1	1, 2, 3, 4

#### 5.1. Effect of $L$

The effects of the CFRP length ( $L$ ), which is determined by the pasted angle, on the interface stresses are investigated. The distributions of the concrete tensile area with different pasted angles of 30°, 60°, 90° and 120° are presented in Figure 8. The gray areas represent when the concrete is compressed, and the other color areas represent when the concrete is tensioned. For the angles of 30, 60° and 90°, the CFRP cannot cover all the concrete tensile areas. According to Figure 9a, the radial tensile stress concentration appears at the edges of the reinforced areas in these three cases. However, for the angle of 120°, all the concrete tensile areas can be completely covered by CFRP, and the interface at the

edges of the reinforced areas is radial compressed. The maximum radial tensile stress is 0.014 MPa, which is much smaller than those in the three previous cases. For the full-pasted case ( $180^\circ$ ), the interface radial tensile stresses mainly appear at the crown and bottom, and the maximum radial tensile stress is 0.013 MPa. It indicates that when the pasted angle is larger than  $120^\circ$ , the maximum radial tensile stress cannot be effectively decreased by extending the pasted length of CFRP.

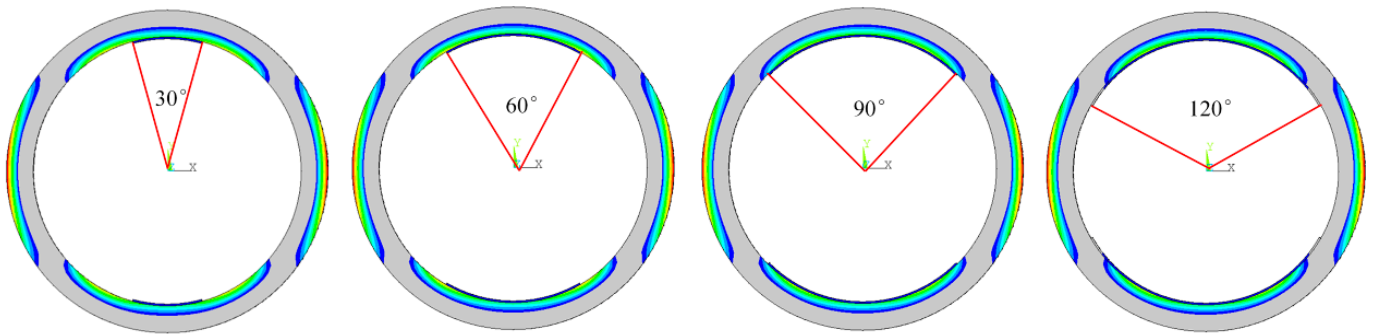


Figure 8. Concrete tensile areas and pasted angles.

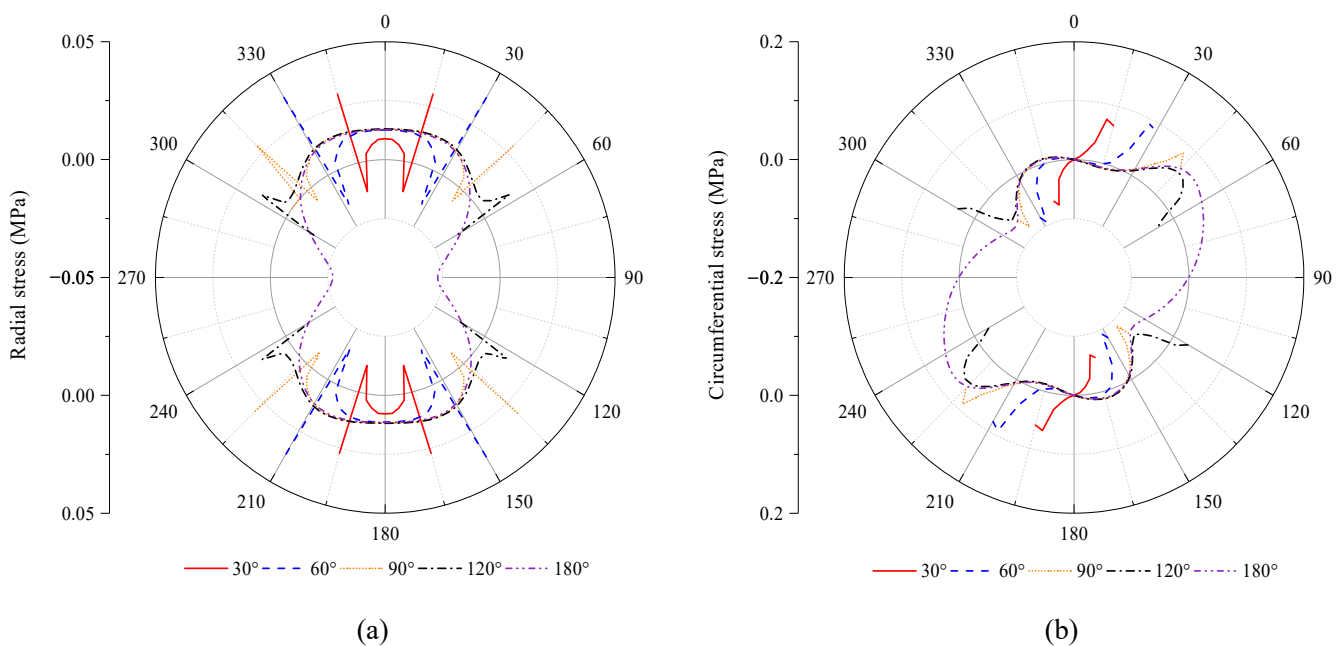


Figure 9. Effect of  $L$  on the reinforced interface stresses: (a) radial stress; (b) circumferential stress.

According to Figure 9b, for the angles of  $30^\circ$ ,  $60^\circ$  and  $90^\circ$ , the maximum circumferential stresses all appear near the edges of the reinforced areas. Since these positions are radial tensioned in Figure 9a, the interface peel failure is most likely to occur there. For the angles of  $120^\circ$ , with the further extension of the CFRP pasted length, the distribution of the interface circumferential stress was effectively improved, and the maximum circumferential stress was significantly decreased. For the full pasted case ( $180^\circ$ ), the curve of the circumferential stress distribution was further smoothed, and the maximum circumferential stress was close to that in the case of  $120^\circ$ .

In total, for a circular tunnel partially reinforced with CFRP, the interface peel failure is most likely to occur near the edges of the reinforced areas. However, the interface radial stresses and circumferential stresses can be effectively decreased by extending the pasted length of CFRP to a certain extent. Therefore, to prevent the peeling failure, the pasted

length of CFRP should be large enough to at least cover all the concrete tensile areas. In this studied case, to save CFRP materials, the pasted angle of 120 is more appropriate.

### 5.2. Effect of $n$

The effects of the CFRP layer ( $n$ ) on the interface stresses are investigated. According to Figure 10, the interface stresses are significantly affected by  $n$ . With the increase in  $n$  from 1 to 3, the maximum radial tensile stress increases by 187%, and the maximum circumferential stress increases by 93%. In addition, pasting multiple layers of CFRP is not conducive to the full immersion of adhesive in CFRP. Therefore, for the partially pasted CFRP reinforcement scheme, decreasing the CFRP layers as much as possible is suggested when it can meet the condition of structural safety.

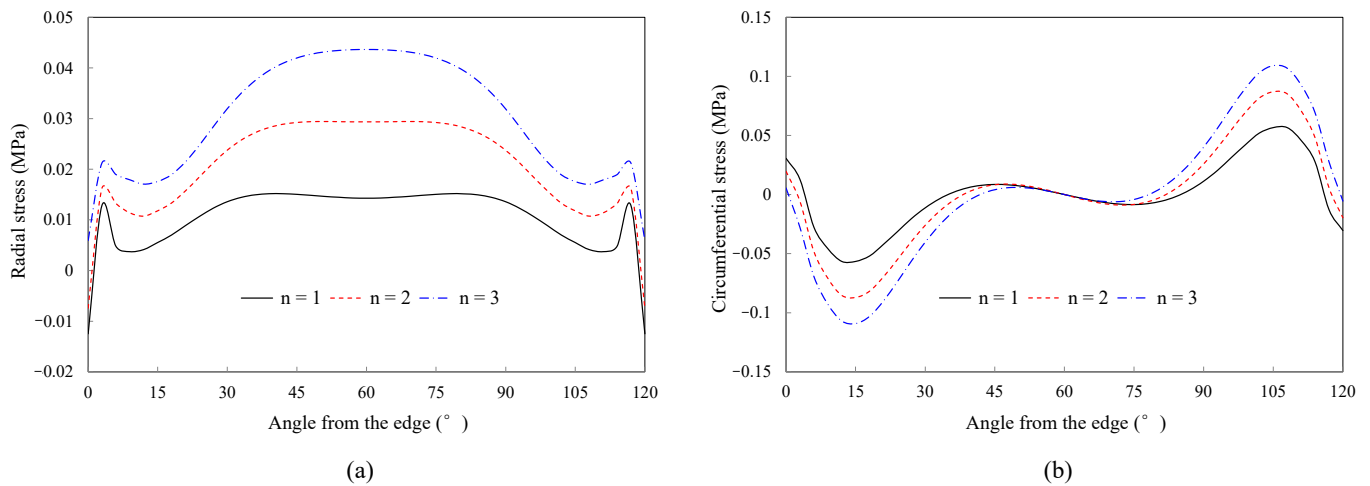


**Figure 10.** Effect of  $n$  on the reinforced interface stresses: (a) radial stress; (b) circumferential stress.

### 5.3. Effect of $t_c$

The effects of the CFRP thickness ( $t_c$ ) on the interface stresses are investigated. According to Figure 11, the interface radial stresses and circumferential stresses are significantly affected by  $t_c$ . With the increase in  $t_c$  from 0.1 mm to 0.2 mm, the maximum radial tensile stress increases by 58%, and the maximum circumferential stress increases by 37%. Therefore, for the partially pasted CFRP reinforcement scheme, decreasing the CFRP thickness can improve the stress state of the interface.

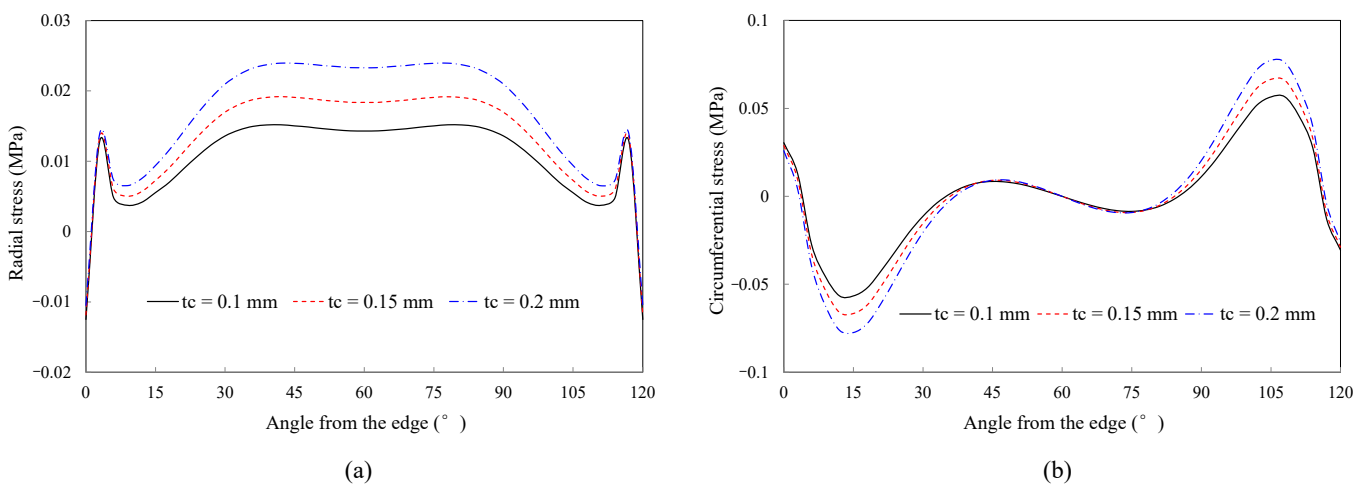


**Figure 11.** Effect of  $t_c$  on the reinforced interface stresses: (a) radial stress; (b) circumferential stress.

#### 5.4. Effect of $E_c$

The effects of the CFRP elastic modulus ( $E_c$ ) on the interface stresses are investigated. According to Figure 12, the interface radial stresses and circumferential stresses are significantly affected by  $E_c$ . With the increase in  $E_c$  from 100 GPa to 500 GPa, the maximum radial tensile stress increases by approximately 150%, and the maximum circumferential stress increases by approximately 131%. Normally, the elastic modulus of the high strength CFRP is approximately 235 GPa, and the elastic modulus of the high modulus CFRP ranges from 345 GPa to 690 GPa. Although the high modulus CFRP has the advantages of good bearing performance and preventing crack propagation, it is detrimental to the long-term combined work of the lining concrete and CFRP.

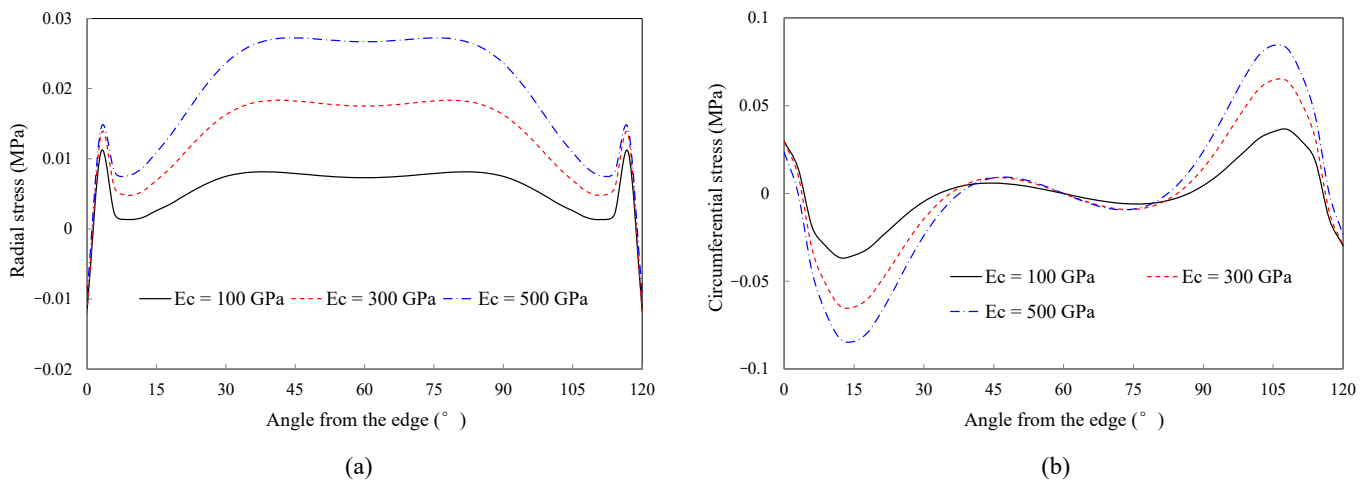


**Figure 12.** Effect of  $E_c$  on the reinforced interface stresses: (a) radial stress; (b) circumferential stress.

#### 5.5. Effect of $t_a$

The effects of the adhesive layer thickness ( $t_a$ ) on the interface stresses are investigated. According to Figure 13, the interface radial stresses are significantly affected by  $t_a$ . With the increase in  $t_a$  from 1 mm to 4 mm, the radial stresses near the central and marginal position of the interface are obviously increased, and the maximum radial tensile stress increases by 39%. However, according to Figure 13b,  $t_a$  has a negligible effect on the interface circumferential stresses. With increasing  $t_a$ , the maximum circumferential stress increases by only 18%. Therefore, for the partially pasted CFRP reinforcement scheme, decreasing the adhesive layer thickness is suggested to decrease the interface radial tensile stress and prevent peel failure.

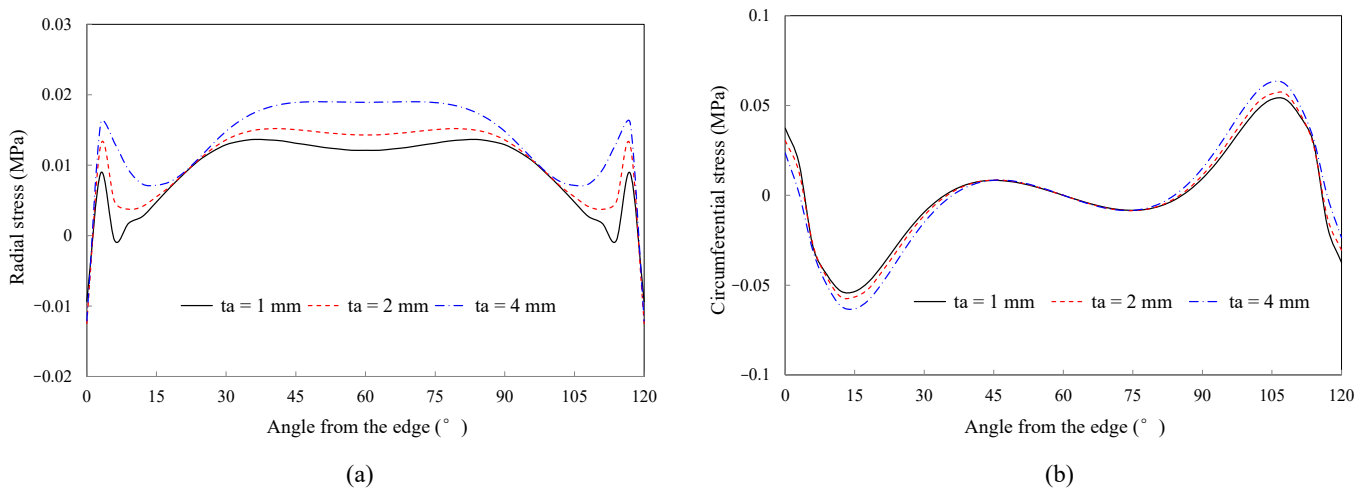


**Figure 13.** Effect of  $t_a$  on the reinforced interface stresses: (a) radial stress; (b) circumferential stress.

### 5.6. Effect of $E_a$

The effects of the adhesive elastic modulus ( $E_a$ ) on the interface stresses are investigated. According to Figure 14, the interface radial stresses and circumferential stresses are significantly affected by  $E_a$ . When  $E_a$  is 0.24 GPa, the distributions of the interface radial stresses and circumferential stresses are relatively uniform. However, with increasing  $E_a$ , the interface stress concentration tends to be obvious. With the increase in  $E_a$  from 0.24 GPa to 11.2 GPa, the maximum radial tensile stress increases by 80%, and the maximum circumferential stress increases by 136%. Therefore, for the partially pasted CFRP reinforcement scheme, decreasing the adhesive elastic modulus has the advantage of preventing interface stress concentration.

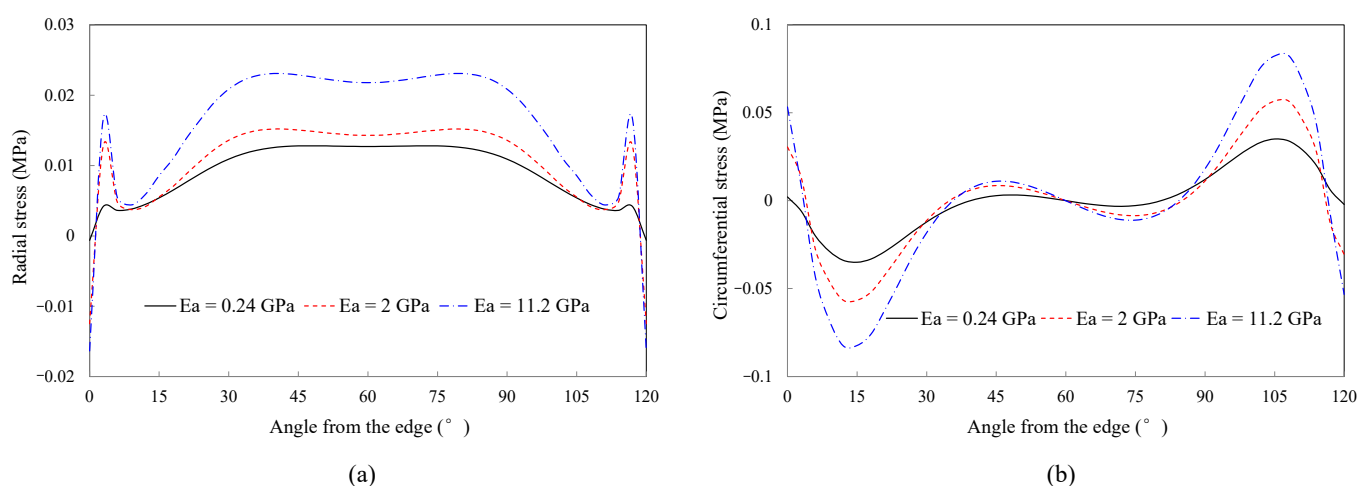


**Figure 14.** Effect of  $E_a$  on the reinforced interface stresses: (a) radial stress; (b) circumferential stress.

## 6. Conclusions

An analytical model is proposed for the curved reinforced interface with the consideration of the interface bond–slip relationship, and a 3D numerical model is established to further investigate the effects of some important parameters. According to the analytical and numerical results, the following conclusions were obtained.

- (1) The analytical results reveal that the interface curvature has a significant effect on the interface radial stresses. With decreasing the radius of the curvature, the interface radial stresses increase significantly.
- (2) The numerical results reveal that the reinforced curved interface stresses are mainly affected by the CFRP's length, layer, thickness, elastic modulus, and the adhesive's thickness, elastic modulus. In engineering practice, these reinforcement parameters should be optimized to decrease the interface stresses and prevent premature peel failure of the structure.
- (3) For the adhesive, decreasing the elastic modulus and thickness of the adhesive layer can significantly improve the stress state of the reinforced interface. For the CFRP, on the premise of meeting the structural bearing requirements, the pasted length of CFRP should be large enough to at least cover all the concrete tensile areas, and the CFRP with smaller thickness, smaller elastic modulus and fewer layers is conducive to the full utilization of materials and long-term combined work of the concrete and CFRP.

As the results of this study, the factors that affect the performance of the tunnel reinforced with CFRP are complex and diverse. This paper preliminarily reveals the influence law of the involved parameters. Multitudinous calculations and orthogonal test analysis should be conducted to further investigate the influence degrees and thresholds of these parameters under various conditions.

**Author Contributions:** Conceptualization, F.Y.; methodology, F.Y.; software, F.Y. and G.Q.; validation, F.Y. and G.Q.; formal analysis, F.Y. and G.Q.; investigation, F.Y. and G.Q.; resources, W.L.; data curation, F.Y. and G.Q.; writing—original draft preparation, F.Y., G.Q., K.L., F.X. and W.L.; writing—review and editing, F.Y., G.Q., K.L., F.X. and W.L.; visualization, F.Y.; supervision, W.L.; project administration, F.Y. and W.L.; funding acquisition, F.Y. and W.L. All authors have read and agreed to the published version of the manuscript.

**Funding:** This research was funded by the National Key Research and Development Program of China (Grant No. 2019YFC0810702), the Fundamental Research Funds for the Central Universities (Grant No. JZ2022HGTA0335) and the Natural Science Foundation of Anhui Province (Grant No. 2208085ME153).

**Institutional Review Board Statement:** Not applicable.

**Informed Consent Statement:** Not applicable.

**Data Availability Statement:** Not applicable.

**Conflicts of Interest:** The authors declare no conflict of interest.

## References

- Liu, D.; Huang, H.; Yue, Q.; Xue, Y.; Wang, M. Behaviour of tunnel lining strengthened by textile-reinforced concrete. *Struct. Infrastruct. Eng.* **2015**, *12*, 964–976. [\[CrossRef\]](#)
- Wang, T.-T.; Lee, C.-H. Life-Cycle Design Considerations for Hydraulic Tunnels: Lessons Learned from Inspection and Maintenance Cases. *J. Perform. Constr. Facil.* **2013**, *27*, 796–806. [\[CrossRef\]](#)
- Meier, U.; Deuring, M. *CFRP Bonded Sheets, FRP Reinforcement for Concrete Structures: Properties and Applications*; Elsevier Science Publishers: Amsterdam, The Netherlands, 1993.
- Zeng, J.-J.; Liao, J.; Ye, Y.-Y.; Guo, Y.-C.; Zheng, Y.; Tan, L.-H. Behavior of FRP spiral strip-confined concrete under cyclic axial compression. *Constr. Build. Mater.* **2021**, *295*, 123544. [\[CrossRef\]](#)
- Liao, J.J.; Zeng, J.J.; Gong, Q.M.; Quach, W.M.; Gao, W.Y.; Zhang, L. Design-oriented stress-strain model for FRP-confined ultra-high performance concrete (UHPC). *Constr. Build. Mater.* **2022**, *318*, 126200. [\[CrossRef\]](#)
- Liao, J.J.; Zeng, J.J.; Chen, J.; Li, J.X.; Yuan, J.S. Stress-strain behavior and design-oriented model for FRP spiral strip-confined concrete. *Compos. Struct.* **2022**, *293*, 115747. [\[CrossRef\]](#)
- Wang, Q.; Zhu, H.; Su, W.; Du, H.; Chen, D. Fatigue performance of CFRP reinforced pretensioned prestressed beams. *Constr. Build. Mater.* **2022**, *324*, 126509. [\[CrossRef\]](#)
- Hollaway, L.C. A review of the present and future utilisation of FRP composites in the civil infrastructure with reference to their important in-service properties. *Constr. Build. Mater.* **2010**, *24*, 2419–2445. [\[CrossRef\]](#)
- Mugahed Amran, Y.H.; Alyousef, R.; Rashid, R.S.M.; Alabduljabbar, H.; Hung, C.-C. Properties and applications of FRP in strengthening RC structures: A review. *Structures* **2018**, *16*, 208–238. [\[CrossRef\]](#)
- Qin, G.; Yang, F.; Jin, D. Stress Transferring Mechanism of a Pressure Tunnel Lining Strengthened with CFRP. *Lat. Am. J. Solids Struct.* **2021**, *18*, 405–423. [\[CrossRef\]](#)
- Yao, J.; Teng, J.; Chen, J. Experimental study on FRP-to-concrete bonded joints. *Compos. Part B Eng.* **2004**, *36*, 99–113. [\[CrossRef\]](#)
- Dai, J.; Ueda, T.; Sato, Y. Development of the Nonlinear Bond Stress–Slip Model of Fiber Reinforced Plastics Sheet–Concrete Interfaces with a Simple Method. *J. Compos. Constr.* **2005**, *9*, 52–62. [\[CrossRef\]](#)
- Cao, S.Y.; Chen, J.F.; Pan, J.W.; Sun, N. ESPI Measurement of Bond-Slip Relationships of FRP-Concrete Interface. *J. Compos. Constr.* **2007**, *11*, 149–160. [\[CrossRef\]](#)
- Cui, E.; Jiang, S.; Wang, J.; Zeng, X. Bond behavior of CFRP-concrete bonding interface considering degradation of epoxy primer under wet-dry cycles. *Constr. Build. Mater.* **2021**, *292*, 123286. [\[CrossRef\]](#)
- Neubauer, U.; Rostasy, F.S. Bond failure of concrete fiber reinforced polymer plates at inclined cracks-experiments and fracture mechanics model. In Proceedings of the 4th International Symposium on Fiber Reinforced Polymer Reinforcement for Reinforced Concrete Structures ACI, Farmington Hills, MI, USA, 1 August 1999; pp. 369–382.
- Monti, M.; Renzelli, M.; Luciani, P. FRP adhesion in uncracked and cracked concrete zones. In *Fiber-Reinforced Polymer Reinforcement for Concrete Structures: Proceeding of the 6th International Symposium on FRP Reinforcement for Concrete Structures, Singapore, 8–10 July 2003*; World Scientific Publications: Singapore, 2003; pp. 183–192.
- Nakaba, K.; Toshiyuki, K.; Tomoki, F.; Yoshizawa, H. Bond behavior between fiber-reinforced polymer laminates and concrete. *ACI Struct. J.* **2001**, *98*, 359–367.
- Savioa, M.; Farracuti, B.; Mazzotti, C. Non-linear bond-slip law for FRP-concrete interface. In *Fiber-Reinforced Polymer Reinforcement for Concrete Structures: Proceeding of the 6th International Symposium on FRP Reinforcement for Concrete Structures, Singapore, 8–10 July 2003*; World Scientific Publications: Singapore, 2003; pp. 163–172.
- Roberts, T.M. Approximate analysis of shear and normal stress concentrates in the adhesive layer of Plated RC Beams. *Struct. Eng.* **1989**, *67*, 222–233.

20. Roberts, T.M.; Haji-Kazemi, H. Theoretical study of the behavior of reinforced concrete beams strengthened by externally bonded steel plates. *Proc. Inst. Civ. Eng.* **1989**, *87*, 39–55.
21. Vilnay, O. The analysis of reinforced concrete beams strengthened by epoxy bonded steel plates. *Int. J. Cem. Compos. Light. Concr.* **1988**, *10*, 73–78. [[CrossRef](#)]
22. Liu, Z.H.; Zhu, B.L. Analytical solutions for R/C beams strengthened by externally bonded steel plates. *J. Tongji Univ.* **1994**, *22*, 21–26.
23. Täljsten, B. Strengthening of beams by plate bonding. *J. Mater. Civ. Eng.* **1997**, *9*, 206–212. [[CrossRef](#)]
24. Malek, A.M.; Saadatmanesh, H.; Ehsani, M.R. Prediction of failure load of R/C beams strengthened with FRP plate due to stress concentration at the plate end. *ACI Struct. J.* **1998**, *95*, 142–152.
25. Rabinovich, O.; Frostig, Y. Closed-Form High-Order Analysis of RC Beams Strengthened with FRP Strips. *J. Compos. Constr.* **2000**, *4*, 65–74. [[CrossRef](#)]
26. Shen, H.S.; Teng, J.G.; Yang, J. Interfacial stresses in beams and slabs bonded with thin plate. *J. Eng. Mech.* **2001**, *127*, 399–406.
27. Monti, G.; Liotta, M. Tests and design equations for FRP-strengthening in shear. *Constr. Build. Mater.* **2007**, *21*, 799–809. [[CrossRef](#)]
28. Wang, J.; Zhang, C. A three-parameter elastic foundation model for interface stresses in curved beams externally strengthened by a thin FRP plate. *Int. J. Solids Struct.* **2010**, *47*, 998–1006. [[CrossRef](#)]
29. Lu, X.Z. Study on FRP-Concrete Interface. Ph.D. Thesis, Tsinghua University, Beijing, China, 2004.
30. Lorenzis, L.D.; Zavarise, G. Interfacial stress analysis and prediction of debonding for a thin plate bonded to a curved substrate. *Int. J. Non-Linear Mech.* **2009**, *44*, 358–370. [[CrossRef](#)]
31. Wang, L.Y. The Experimental Study on Pressure Conduit of Ferroconcrete Reinforced by Fabric Reinforced Plastic. Master's Thesis, Wuhan University, Wuhan, China, 2004.
32. Hugo, C.B.; Carlos, C.; Manuel, A.G.S. linear and nonlinear analysis of bond slip models for interfaces between FRP composites and concrete. *Compos. Part B* **2013**, *45*, 1554–1568.
33. Obaidat, Y.T.; Heyden, S.; Dahlblom, O. Evaluation of Parameters of Bond Action between FRP and Concrete. *J. Compos. Constr.* **2013**, *17*, 626–635. [[CrossRef](#)]
34. Furtado, A.; Rodrigues, H.; Arêde, A.; Varum, H. Experimental tests on strengthening strategies for masonry infill walls: A literature review. *Constr. Build. Mater.* **2020**, *263*, 120520. [[CrossRef](#)]
35. Liu, Y.; Dong, A.; Zhao, S.; Zeng, Y.; Wang, Z. The effect of CFRP-shear strengthening on existing circular RC columns under impact loads. *Constr. Build. Mater.* **2021**, *302*, 124185. [[CrossRef](#)]